

A EUROPEAN JOURNAL OF CHEMICAL BIOLOGY

CHEM **BIO** CHEM

SYNTHETIC BIOLOGY & BIO-NANOTECHNOLOGY

Accepted Article

Title: Towards Catalytic Antibiotics: Redesign of Aminoglycosides to Catalytically Disable Bacterial Ribosome

Authors: Boris Smolkin, Alina Vilensky, Tomasz Pieńko, Michal Shavit, Valery Belakhov, Joanna Trylska, and Timor Baasov

This manuscript has been accepted after peer review and appears as an Accepted Article online prior to editing, proofing, and formal publication of the final Version of Record (VoR). This work is currently citable by using the Digital Object Identifier (DOI) given below. The VoR will be published online in Early View as soon as possible and may be different to this Accepted Article as a result of editing. Readers should obtain the VoR from the journal website shown below when it is published to ensure accuracy of information. The authors are responsible for the content of this Accepted Article.

To be cited as: *ChemBioChem* 10.1002/cbic.201800549

Link to VoR: <http://dx.doi.org/10.1002/cbic.201800549>

WILEY-VCH

www.chembiochem.org

A Journal of



Towards Catalytic Antibiotics: Redesign of Aminoglycosides to Catalytically Disable Bacterial Ribosome

Boris Smolkin,^[a] Alina Khononov,^[a] Tomasz Pieńko,^[b,c] Michal Shavit,^[a] Valery Belakhov,^[a] Joanna Trylska^[b] and Timor Baasov^{*[a]}

Dedicated to Professor Chi-Huey Wong on the occasion of his 70th birthday.

Abstract: The emergence of multidrug-resistant pathogens that are resistant to the majority of currently available antibiotics is a significant clinical problem. The development of new antibacterial agents and novel approaches is therefore extremely important. We set out to explore the potential of catalytic antibiotics as a new paradigm in antibiotics research. Here we describe our pilot study on the design, synthesis, and biological testing of a series of new derivatives of the natural aminoglycoside antibiotic neomycin B for their potential action as catalytic antibiotics. The new derivatives showed significant antibacterial activity against wild-type bacteria and were especially potent against resistant and pathogenic strains including *P. aeruginosa* and MRSA. Selected compounds displayed RNase activity even though the activity was not as high and specific as we would have expected. Based on the observed chemical and biochemical data, along with the comparative molecular dynamics simulations of the prokaryotic rRNA decoding site, we postulate that the rational design of the catalytic antibiotics should involve not only their structure but also a comprehensive analysis of the rRNA A-site dynamics.

1. Introduction

The ongoing emergence of multidrug-resistant pathogens requires continuous intensive search for novel antibiotics. Unfortunately, only two new classes of antibiotics, oxazolidinones^[1] and lipopeptides^[2] have been introduced into clinical practice during the last decades. Furthermore, it has been well documented that once a new antibiotic is introduced into the clinic, whether it is a novel chemical entity acting at a distinct

bacterial target or a semisynthetic derivative that counters the resistance to its parent drug, within only a short matter of time new resistance will emerge and create a serious public health problem^[3]. Some bacterial strains have developed multi-drug resistance that covers the majority of currently available antibiotics. The significance of this health problem has re-energized the search for new antibacterial agents and novel approaches.

One innovative approach is the development of catalytic antibiotics: the pharmacophore of an existing antibiotic is modified to include a catalytic warhead that disables the target in a catalytic manner. Unlike conventional antibiotics that act on their targets either in a reversible (non-covalent interaction) or irreversible manner (covalent interaction), the antibiotics acting in a catalytic manner promote multiple turnovers of a catalytic cycle. The possible benefits include: (i) activity at lower dosages and consequently reduced side effects, (ii) activity against drug-resistant bacteria, and (iii) reduced potential for generating new resistance.

In general, the idea of catalytic drugs is not novel and several studies towards the development of such agents have been reported previously^[4,5]. These include numerous peptide-cleaving agents based on small molecule metal complexes as artificial proteases^[4], site-specific RNA-cleaving agents that combine a reactive moiety (phosphodiester cleavage directed non-metallic, warhead) with a recognition element (sequence-specific hybridization to target RNA)^[6], and non-metallic small organic molecules as artificial ribonucleases^[7,8].

Inspired by these findings, we set out to explore the potential of catalytic antibiotics as a new paradigm in antibiotics research. Herein we focus on redesigning aminoglycosides, which represent a particularly well-studied and broad-spectrum class of antibiotics. These molecules exert their therapeutic (bactericidal) effect by selectively binding to the aminoacyl-tRNA binding site (A-site) of the bacterial 16S rRNA, thereby interfering with translational fidelity during protein synthesis^[9]. Previous reports on the ability of copper-aminoglycoside complexes to promote hydrolytic and oxidative cleavage of RNA^{[10][11][12][13]} have prompted the potential use of these complexes as metallo-drugs with potent antibacterial activity. However, antibacterial tests showed no significant enhancement in the activity of the copper-aminoglycoside complex compared to the parent aminoglycoside^[14], suggesting that a more sophisticated design process is needed to obtain a biologically functional catalytic antibiotic.

[a] Dr. B. Smolkin, A. Khononov, Dr. M. Shavit, Dr. V. Belakhov, Prof. Dr. T. Baasov

The Edith and Joseph Fischer Enzyme Inhibitors Laboratory,
Schulich Faculty of Chemistry Department
Technion - Israel Institute of Technology
Haifa 3200003, Israel

E-mail: chtimor@technion.ac.il

[b] Dr. T. Pieńko, Prof. Dr. J. Trylska

Centre of New Technologies
University of Warsaw
Banacha 2c, 02-097 Warsaw, Poland

[c] Dr. T. Pieńko

Department of Drug Chemistry, Faculty of Pharmacy with the
Laboratory Medicine Division
Medical University of Warsaw
Banacha 1a, 02-097 Warsaw, Poland

Supporting information for this article is given via a link at the end of the document.

FULL PAPER

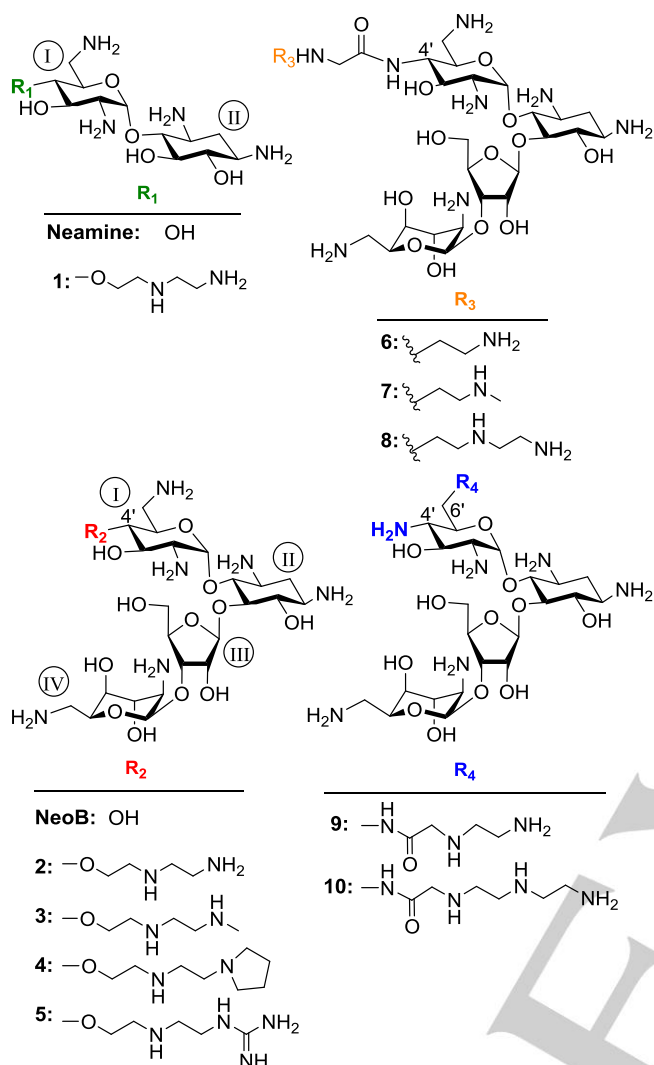


Figure 1. Structures of neamine, neomycin B (NeoB) and synthetic aminoglycosides 1-10 that were investigated in this study.

We hypothesized that by employing the available structural and mechanistic library of data on the aminoglycoside target, natural ribonuclease systems, and recently reported artificial, small molecule systems capable of cleaving phosphodiester bonds, we could create a new variant of aminoglycoside antibiotic that would *selectively and catalytically* act on the bacterial ribosome and irreversibly deactivate it. To test this hypothesis, herein we describe our pilot studies on the design, synthesis and biological evaluation of a series of new Neomycin B (NeoB) derivatives (compounds 1-10, Figure 1) substituted at the 4' position (via ether and amide linkages) or at the 6' position (via amide linkage) with various diamine moieties as potential catalytic warheads for the hydrolysis of rRNA. The observed data demonstrates that most of the new derivatives retain the antibacterial potency of the parent NeoB against wild-type strains of both Gram-negative and Gram-positive bacteria and display significantly better activity against the tested resistant strains.

Particularly improved activities were observed against Methicillin-resistant *Staphylococcus aureus* (MRSA) and *Pseudomonas aeruginosa* strains, which are both highly resistant to conventional aminoglycosides. Interestingly, three of the 4'-amide derivatives showed a 2-fold stronger inhibition of protein synthesis in comparison to NeoB and other clinically used aminoglycosides. However, all attempts to demonstrate the cleavage of the scissile phosphodiester bond of rRNA by these derivatives have been unsuccessful. Based on the observed chemical and biochemical data, along with the comparative molecular dynamics simulations of the prokaryotic rRNA decoding site, we postulate that the rational design of the catalytic antibiotics should involve not only their structure but also a comprehensive analysis of the rRNA A site dynamics.

2. Results and Discussion

2.1. Design hypothesis

Initially, we considered the following three key aspects in our design of a potential aminoglycoside catalyst: (1) the choice of the phosphodiester bond in the A site that should be the most susceptible to catalytic cleavage, (2) the potential “catalytic warhead” structures and (3) the attachment site of a “catalytic warhead” on the aminoglycoside structure.

(1) *The choice of the phosphodiester bond.* Compelling evidence is now available that the successful cleavage of an RNA phosphodiester bond requires substantial motion in the HO-C2'-C3'-O-P bonds of the ribose-3'-phosphate region to reach the necessary low energy transition state wherein the C2'-OH group is orientated for in-line nucleophilic attack on the scissile bond^[7]. Such flexibility is usually achieved by the enzyme-induced flipping of the base attached to the RNA scissile bond. The mechanisms suggested for the RNase T1^[15], RNase α -sarcin^[16], and for several ribozymes^[17], are only a few of the examples that support this notion. Of particular relevance is the proposed mechanism for colicin E3 (ColE3), a natural enzymatic toxin produced in several *E. coli* strains, that selectively cleaves a phosphodiester bond between A1493 and G1494 of 16S rRNA^[18]. This cleavage impairs the protein translation process and consequently leads to cell death. The proposed mechanism of ColE3 also explains why this natural ribonuclease cleaves the specific position in the A site of rRNA, between A1493 and G1494. This region of the A site is very important functionally (for correct proofreading) and is also one of the most flexible and accessible regions in the whole ribosome because it needs to accommodate the incoming aminoacyl-tRNA.

Consequently, we postulated that the target phosphodiester bond must be within the region of rRNA that upon binding of an aminoglycoside undergoes the most extensive conformational change. Moreover, this region is virtually the same as that of ColE3 binding: G1491-A1492-A1493-G1494. Since the binding of most aminoglycosides induces extensive flipping of A1492 and A1493 base residues from the bulged-in (ligand unbound ribosome) to the bulged-out conformation^[19], similar to that of the ColE3 binding^[20], it is most likely that the best three

For internal use, please do not delete. Submitted_Manuscript

FULL PAPER

phosphodiester bond candidates within the A-site are between G1491-A1492, A1492-A1493, and A1493-G1494.

(2) The choice of the catalytic warheads. Previous studies with simple diamines have demonstrated their ability to accelerate the cleavage of adenylyl(3'-5')-adenosine (ApA), from one to three orders of magnitude more efficiently than the corresponding monoamines^{[21],[22]}. Furthermore, it has been shown that the order of reactivity for the simple diamine series is as follows: N-2-N > N-3-N > N-1-N > N-4-N > N-5-N. The strong activities of N-2-N and N-3-N were primarily ascribed to the abundance of catalytically active monocations (61% for N-2-N and 7.4% for N-3-N) that exist at pH 7 because the second protonation is suppressed due to the electrostatic repulsion of the positively charged ammonium ions (the corresponding pK_a 's are 6.8 and 9.4 for N-2-N, and 8.1 and 9.8 for N-3-N). Based on these observations, we selected ethylenediamine, methyl ethylenediamine, diethylenetriamine, N-(2-aminoethyl)pyrrolidine and guanidine-ethyleneamine as potential "catalytic warheads" and prepared the new NeoB derivatives **1-10** (Figure 1).

(3) The choice of the attachment site of a catalytic warhead. We selected the 4'-hydroxyl group (ring I) of NeoB (Figure 2) as the attachment site for the following reasons. Firstly, the available structural data on the interaction of NeoB with its ribosomal target^[19] indicate that the 4'-hydroxyl is positioned in front of the scissile phosphodiester bond of G1491-A1492, and is near a large cavity formed in the A-site that makes its modification feasible. Secondly, our preliminary molecular modelling studies of the proposed warheads linked at the 4' position suggested that the phosphodiester bond between G1491 and A1492 is the closest one and its cleavage is feasible through acid-base catalysis (Figure 2): the terminal amino group in its ammonium form can activate the phosphate between G1491 and A1492 as a general-acid (3.9 Å distance), and the next nearest amine can activate the 2'-hydroxyl of G1491 as a general-base (2.6 Å distance). Finally, Ye and co-workers have recently reported a series of new derivatives of kanamycin B, modified at the 4'-OH position, which show excellent antibacterial activity against both wild-type and resistant bacteria^[23]. The following findings of this study are of particular importance: (1) the side-chain free amine is best tolerated by the ribosome; (2) the A-site of the ribosome can accommodate bulky substituents linked at the 4'-position. Based upon these collective data, we selected the 4'-OH group (ring I) of NeoB as an attachment site for the catalytic warhead and the G1491-A1492 as the cleavage site, as schematically illustrated in Figure 2.

2.2. Synthesis of 4'-O-linked compounds

To selectively modify NeoB at the desired 4' position, we initially developed the required synthetic pathway for its simplest fragment neamine, which consists of rings I and II of NeoB, and prepared the derivative **1** as illustrated in Scheme 1. The synthesis started from the commercial paromomycin sulfate, which was treated with anhydrous HCl (AcCl in MeOH) at reflux to give a highly regioselective hydrolysis between the rings II and III, and afforded paromamine as its hydrochloride salt. The observed salt was converted to the free base form by passing it through a column of Dowex 50W (H⁺ form). Paromamine in its

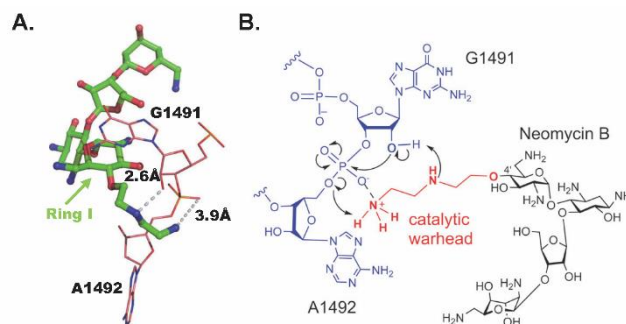


Figure 2. (A) Ball and stick representation of compound **2**-induced cleavage site in the bacterial rRNA A-site. Modelling has been performed by superimposition of **2** with NeoB structure in the crystal structure of NeoB bound to the rRNA oligonucleotide model (PDB ID 2ET4)^[19] by using PyMol. (B) Proposed catalytic action of compound **2** on the hydrolysis of the phosphodiester bond between G1491 and A1492. Modelling has been performed by superimposition of **2** structure with Neomycin A-site crystal structure (PDB ID 2ET4) by using PyMol.

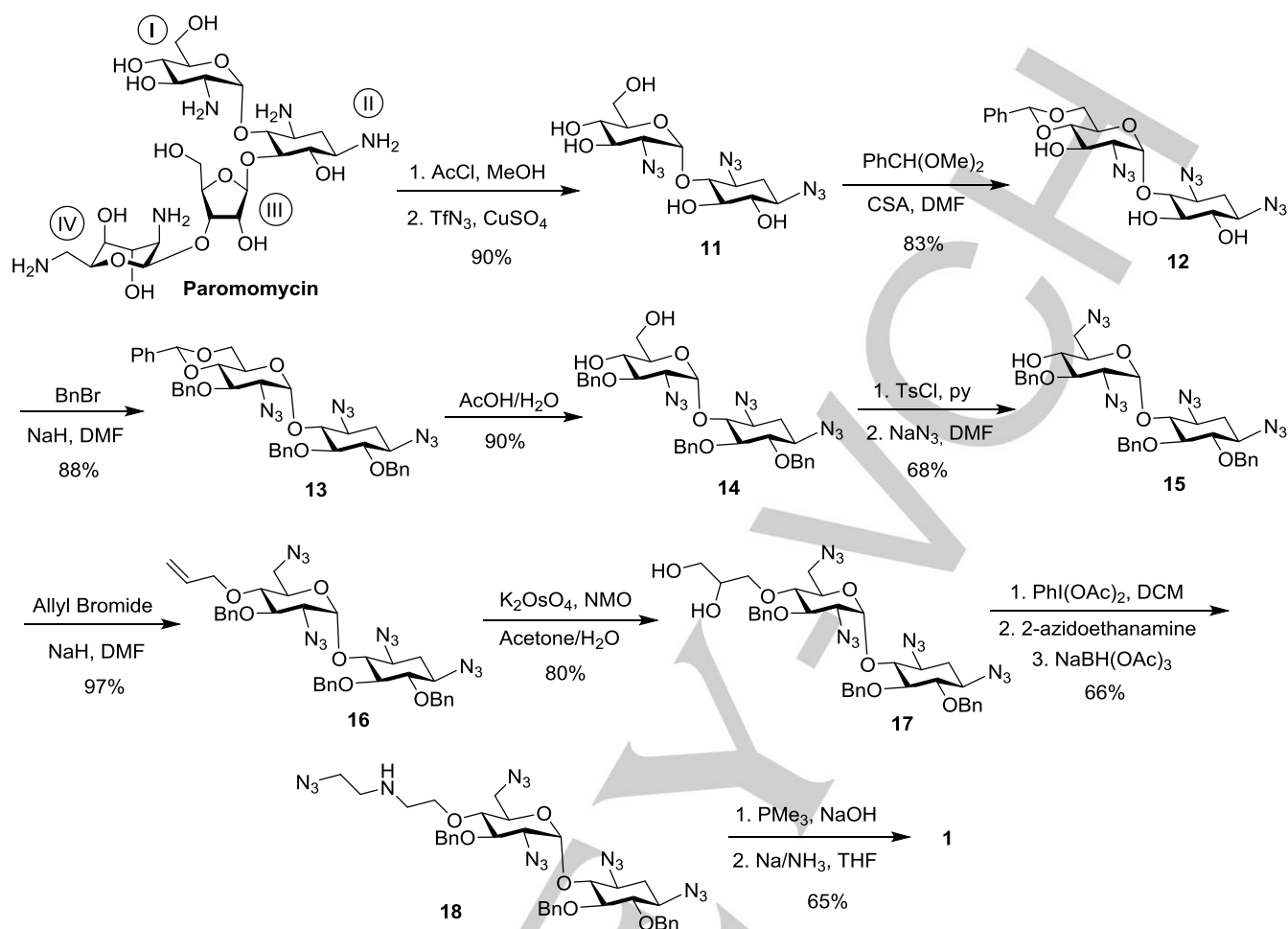
free base form was then converted to the corresponding perazido derivative **11** by the diazo transfer reaction in the presence of TfN₃, CuSO₄·5H₂O and Et₃N.

Treatment of **11** with benzaldehyde dimethylacetal in dry DMF in the presence of camphor sulfonic acid (CSA) afforded the corresponding benzylidene acetal **12**, which was then O-benzylated with benzyl bromide (BnBr) in the presence of NaH in DMF to yield the tribenzyl ether **13**. Removal of the benzylidene group (acetic acid, 60°C) gave the corresponding diol **14**, which was then selectively tosylated at the 6'-hydroxyl group followed by nucleophilic substitution with sodium azide to yield compound **15**. Allylation of the 4'-hydroxyl with allyl bromide in the presence of NaH in DMF gave the 4'-allyl derivative **16**. Attempts to convert **16** to the corresponding aldehyde by ozonolysis resulted in a mixture of products due to the partial oxidation of the benzyl groups. To solve this problem, the double bond in **16** was first converted to the corresponding diol **17** by using the procedure of Nicolaou^[24]. Oxidative cleavage of the diol **17** [PhI(OAc)₂, DCM] was followed by in-situ reductive amination with 2-azidoethanamine^[25] to yield the corresponding 4'-azido amine **18** in 66% isolated yield. Finally, after several unsuccessful attempts to remove the benzyl and azide protections in **18**, we found the sequential operation of the Staudinger and Birch reactions to be the best protocol. Thus, the Staudinger reaction (PMe₃, NaOH) followed by the Birch reduction (Na/NH₃, THF) gave the target compound **1** in 65% isolated yield.

The 4'-O-substituted derivatives of NeoB, compounds **2-5** (Figure 1), were synthesized using the same strategy described for the synthesis of compound **1** with some modifications as illustrated in Scheme 2. The modifications used were as follows. Firstly, unlike the azidation of paromamine with TfN₃ to yield the corresponding perazido derivative **11** (Scheme 1), the same reaction on paromomycin gave a very low yield of the desired perazido derivative **19**.^{[26][27]} In an attempt to improve the yield of the desired perazido product, instead of TfN₃ we used the imidazole-1-sulfonyl azide hydrochloride (ImSO₂N₃·HCl)^[28] and

For internal use, please do not delete. Submitted_Manuscript

FULL PAPER



Scheme 1. Chemical transformation of paromomycin into pseudo-disaccharide **1**.

replacement of tosyl chloride with the more bulky tri-isopropylsulfonyl chloride (trityl chloride), which was more selective for the protection of the 6'-hydroxyl (conversion of compound **22** to **23**) and gave 60% yield over two steps (tritylation and azidation).

The common intermediate diol **25** was separately subjected to in-situ oxidation and reductive amination steps with four different amine linkers, compounds A, B, 1-(2-aminoethyl)pyrrolidine and C (see Chart 1)^[25], to afford the corresponding protected 4'-O-derivatives of NeoB, compounds **26-29** (Scheme 2). The Staudinger reaction (PMe₃, NaOH) followed by the Birch reduction (Na/NH₃, THF) gave the target compounds **2-5** in average to modest isolated yields. The structures of all new compounds (**1-5**) were confirmed by combining various 1D and 2D NMR techniques, including 2D ¹H-¹³C HMQC and HMBC, 2D COSY, and 1D selective TOCSY experiments, along with mass spectral analysis.

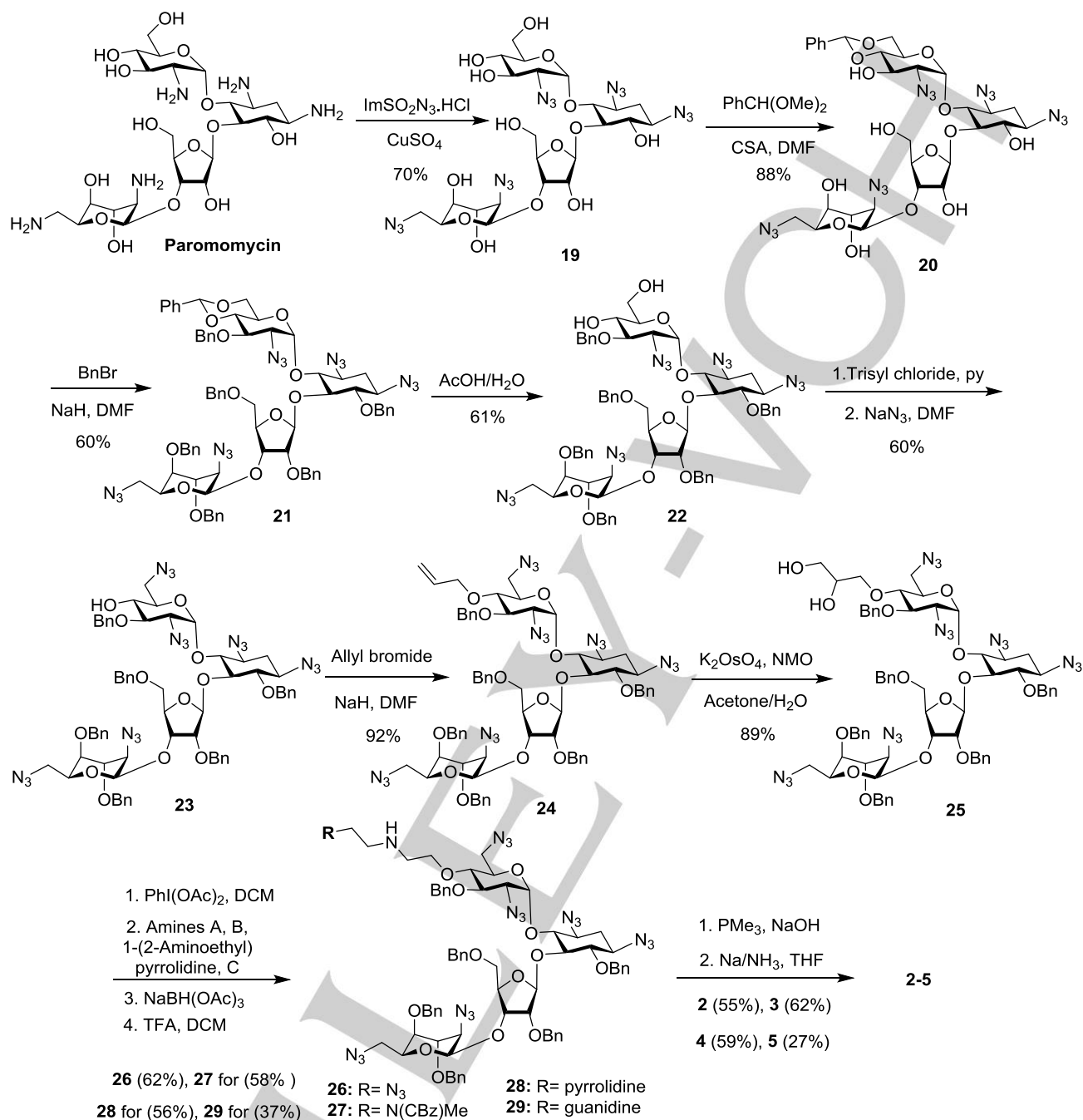
2.3. Synthesis of 4'- and 6'-amide linked compounds

For the synthesis of the 4'-amide derivatives, the alcohol **23** (Scheme 2) was first oxidized with Dess–Martin periodinane (DMP) to form the corresponding 4'-ketone **30**, which was then reduced with sodium borohydride to afford compound **31** with an

axial hydroxyl at the 4' position. Compound **31** was treated with triflic anhydride (Tf₂O, pyridine, CH₂Cl₂) to form the corresponding 4'-triflate, which was then reacted with ammonia in acetone to yield **32** with an equatorial amine at 4' position. Next, **32** was treated with chloroacetyl chloride to give the 4'-chloride **33**, which was then separately reacted with three different amines, compounds A, B, and diethylene triamine, to afford the corresponding 4'-amide derivatives of NeoB in their protected forms (compounds **34**, **35** and **36**, respectively). These products were then deprotected using the two-step procedure described above (Staudinger and Birch), to afford the corresponding 4'-amide derivatives of NeoB, compounds **6**, **7** and **8** in 64%, 68% and 20% isolated yields, respectively. Interestingly, during the last deprotection step (the Birch reduction), we discovered that if this step proceeds in the presence of excess sodium, transamidation rearrangement of the warhead, from the 4' position to the 6' position, takes place. The structure of the rearrangement product (6'-amide) was confirmed by its isolation and subsequent spectral assignment by using a combination of various 1D and 2D NMR techniques (see Figure S1 in Supporting Information). This rearrangement probably occurs due to the strong basic conditions generated after quenching of the reaction, which results in the

For internal use, please do not delete. Submitted_Manuscript

FULL PAPER



Scheme 2. Chemical transformation of paromomycin into synthetic derivatives 2-5.

formation of sodium hydroxide. We exploited this transformation by performing the Birch reaction step under excess sodium, and synthesized the corresponding 6'-amide linked compounds **9** and **10** in 74% and 36% isolated yields, respectively.

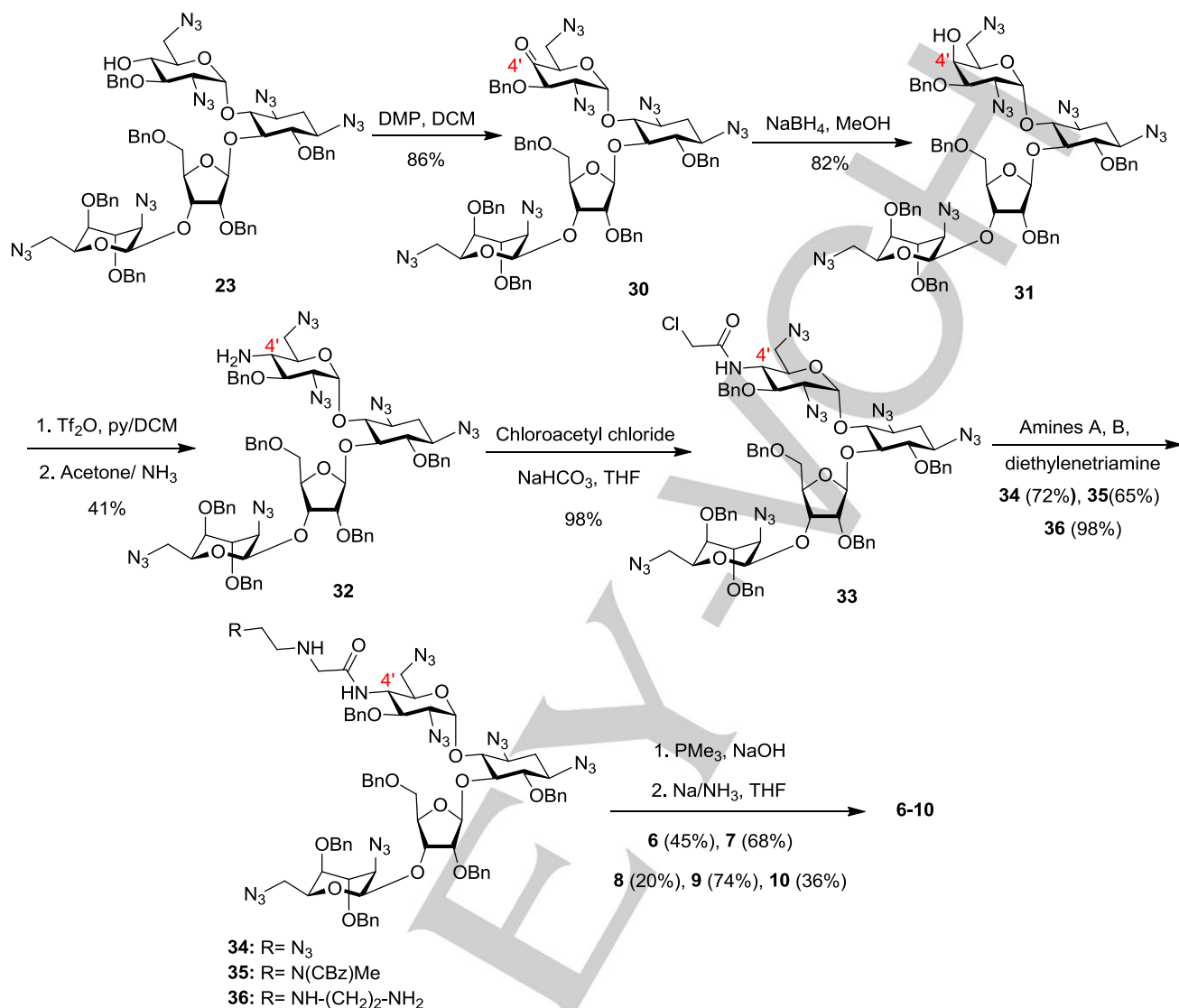
2.4. Antibacterial activity and protein translation inhibition tests

In order to probe the influence of the attached warheads on antibacterial activity, the minimal inhibitory concentration (MIC)

values for the new designer structures **1-10** were determined against wild-type (WT) Gram-negative and Gram-positive bacteria. Although this simple test cannot confirm or disprove catalytic activity, it is nonetheless of the utmost importance as it reveals how the compounds act *in vivo*. Furthermore, we anticipated that unusually low MIC values would be indicative of a high catalytic rate and turnover.

For internal use, please do not delete. Submitted_Manuscript

FULL PAPER



Scheme 3. Chemical transformation of intermediate 23 in to the synthetic derivatives 6-10.

Table 1 shows the comparative MIC values of NeoB and of compounds **1-10** against both Gram-negative and Gram-positive bacteria, including pathogenic and resistant strains. The bacterial strains that were included in these tests were as follows: two WT *E. coli* strains (R477-100 and 25922) as representatives of Gram-negative bacteria with unknown resistance to aminoglycosides^[29] and two WT *Staphylococcus epidermidis* and *Bacillus subtilis* strains as representatives of Gram-positive bacteria (the clinically used aminoglycosides have significant antibacterial activity against these strains).^[30] The resistant strains included Methicillin-resistant *Staphylococcus aureus* (MRSA), a Gram-positive bacterium, whose treatment represents a great challenge in the clinic, the MRSA 252, which is known for its high resistance to aminoglycosides^[31] and the MRSA CI 15877, which is resistant to natural aminoglycosides^[32]. Other pathogens that were tested

included several strains of *Pseudomonas aeruginosa* that have an inherent resistance to aminoglycosides^{[33],[34]}.

The comparative data collected in Table 1 show that all the new derivatives of NeoB, compounds **2-10**, exhibit significant antibacterial activity against both the WT and aminoglycoside-resistant strains including Gram-negative and Gram-positive bacteria. In general, the activity of the novel NeoB derivatives against the WT Gram-negative bacteria is similar to or slightly lower than that of the parent NeoB. The activities against the WT Gram-positive bacteria were diverse across the different strains tested. The activity of most of the compounds against *S. epidermidis* is similar to or better than that of NeoB, while the activity against *B. subtilis* is generally lower than that of NeoB. Interestingly, all new derivatives (compounds **2-10**) have shown significantly improved activity against the Gram-negative strains of pathogenic *P. aeruginosa* in comparison with NeoB.

For internal use, please do not delete. Submitted Manuscript

FULL PAPER

Table 1. Comparative antibacterial activity (MIC values in $\mu\text{g/mL}$) and inhibition of protein translation (IC₅₀ values) in prokaryotic system of NeoB and synthetic compounds **1-10**

Bacteria/ compound	a Gram-negative	b	c Gram-positive	d	e <i>P. aeruginosa</i>	f	g	h MRSA	i	j <i>Geobacillus</i>	k	IC ₅₀ (μM)
NeoB	12	12	6	0.75-1.5	>192	48-96	192	>192	48	0.2	12	0.01±0.002
1	384	>384	192	48	48-96	48-96	48-96	192	48	6	12	2.03±0.3
2	48	48	6	6	24-48	6-12	24	6-12	0.75	0.2	0.8	0.02±0.001
3	96	96	6	6-12	48	12	24	24	3	0.2	0.8	0.03±0.005
4	48	48-96	6	3-6	96	48	48	24	6	0.2	0.8	0.03±0.007
5	192	192	24	12	-	-	-	-	-	-	-	0.08±0.005
6	24	48	6	2	24	6	48	24-48	1.5	0.2	0.4	0.005±0.0005
7	24	24	6	3-6	24	24	48	24	1.5	0.2	0.4	0.07±0.004
8	48	48	3	6	24	24-48	48	12-24	0.75	0.4	1.5	0.07±0.007
9	48	48	6	3-6	48	48-96	24	12	1.5	0.2	0.8	0.006±0.0009
10	24	48	6	3	24	24	48-96	12-24	1.5	0.2	0.4	0.006±0.0009

The shadowed rows in the table highlight the most potent compounds.

[a] *Escherichia coli* R477-100; [b] *Escherichia coli* 25922; [c] *Staphylococcus Epidermidis*; [d] *Bacillus Subtilis*; [e] *Pseudomonas aeruginosa* 1275; [f] *Pseudomonas aeruginosa* 27853; [g] *Pseudomonas aeruginosa* O1; [h] MRSA 252; [i] MRSA 15877; [j] *Geobacillus stearothermophilus* T-1 60°C; [k] *Geobacillus stearothermophilus* KanR 60°C;

P. aeruginosa is a nosocomial human pathogen known to be inherently resistant to aminoglycosides due to the presence of the chromosomally encoded APH(3')-IIb enzyme. This enzyme catalyzes the transfer of the ATP γ -phosphoryl group to the 3'-hydroxyl of many aminoglycosides, rendering them inactive as antibiotics^[34]. The observed improved activity of the new derivatives in comparison to NeoB, against the tested strains of *P. aeruginosa* can be explained by the steric hindrance of the cationic warhead, which introduces unfavorable interactions with the APH(3')-IIb enzyme active site.

A very similar improvement in antibacterial performance of the new designers versus that of NeoB was also observed against the Gram-positive pathogenic MRSA strains. Especially large improvements were observed for compounds **2** and **8**, exhibiting MIC values 64 times lower than that of NeoB. No significant difference in antibacterial activity was observed between the 4'-ether (compounds **1-5**) and 4'-amide (compounds **6-8**) derivatives, even though we had expected the 4'-amide derivatives to be more active because of the potential for additional attractive interactions between the amide bond and the rRNA. Compound **1**, a neamine-based derivative, has a substantially lower antibacterial activity in comparison with the other compounds tested, indicating that its binding affinity to the A-site is much lower.

Since the successful cleavage of an RNA phosphodiester bond requires substantial conformational flexibility, it was important to investigate the possibility that the standard incubation temperature of 37°C is not high enough to allow the "installed warheads" to reach the activation energy required for

the hydrolysis of the scissile phosphodiester bond of rRNA. To test this hypothesis, we decided to test the antibacterial activity against the thermophilic strain *Geobacillus T1* with the optimal growth temperature of 60°C (Table 1). We expected that if the new compound had catalytic activity, it would show better activity than NeoB at 60°C. However, all the new compounds, **1-10**, showed antibacterial activity similar to that of NeoB against the WT *Geobacillus T1*. Against the *Geobacillus T1* harboring the resistance to kanamycin, as expected, most of the new compounds maintained their high antibacterial activity, while NeoB almost lost its activity.

In summary, even though we cannot conclude from the observed comparative MIC data whether or not compounds **1-10** have catalytic activity, we can definitely claim that the modifications we introduced have not hindered the binding to the A-site and most of the derivatives have retained significant antibacterial activity. Moreover, the new compounds have overcome the existing resistance of *P. aeruginosa* and MRSA pathogens to aminoglycosides, which has been one of the greatest challenges in today's antibacterial research!

Next, we tested the protein translation inhibition by determining half-maximum inhibition levels (IC₅₀ values, Table 1). While most of the new compounds show activity in the same order of magnitude as the parent NeoB, compounds **6**, **9** and **10** with a 4'-nitrogen have a 2-fold inhibitory potency compared to NeoB (IC₅₀ values of 0.006, 0.005, 0.006 and 0.01 for **6**, **9**, **10**, and NeoB respectively). This could be explained by the additional interactions of the 4'-amide (compound **6**) and 4'-amine

For internal use, please do not delete. Submitted_Manuscript

FULL PAPER

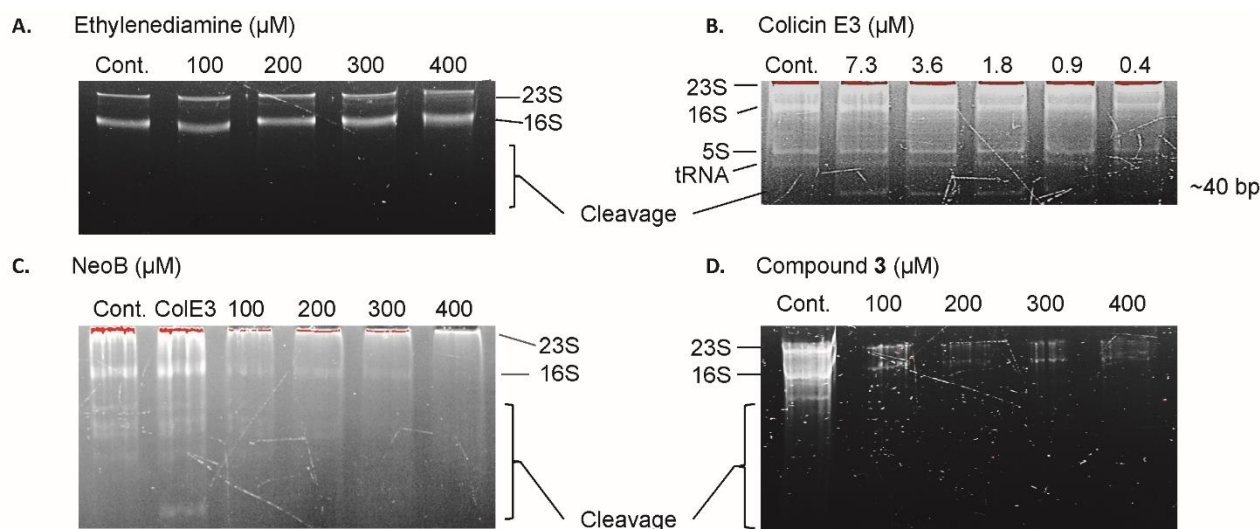


Figure 3. Cleavage experiments of *E. coli* ribosomes in the presence of ethylenediamine, colicin E3, NeoB and compound **3**. A) Lane 1, *E. coli* ribosomes (control). Lanes 2-5, ribosomes treated with increasing concentrations of ethylenediamine. B) Lane 1, (control). Lanes 2-6, ribosomes treated with decreased concentrations of colicin E3. C) Lane 1, (control); Lane 2, ribosomes treated with 7.3 μM colicin E3 (ColE3); Lanes 3-6, ribosomes treated with increasing concentrations of NeoB. D) Lane 1, (control). Lanes 2-4, ribosomes treated with increasing concentrations of compound **3**. rRNA fragments were analyzed on 6% acrylamide TBE/urea gel, stained with syber gold, and analyzed by fluorescence

(compounds **9** and **10**) of these compounds with the ribosomal A-site. However, the increased binding affinity of the compound for the A site may result in its slow dissociation from the ribosome (very small k_{off} value), which would then adversely affect the catalytic performance. To test this possibility, we synthesized compound **1**, which is a smaller analog of compound **2**, as it lacks rings III and IV of NeoB. We found that the inhibition potency of compound **1** ($\text{IC}_{50} = 2.03 \mu\text{M}$, a neamine derivative) is two orders of magnitude lower than the other compounds tested and is one order of magnitude lower than that of the parent neamine scaffold ($\text{IC}_{50} = 0.28 \mu\text{M}$). Thus, it would appear that the neamine pharmacophore is not a suitable choice for the aminoglycoside scaffold unless the catalytic efficiency of the warhead is greatly improved, since the attachment of the warheads has a deleterious effect on the binding affinity at the target.

2.5. RNase activity tests

Since compounds **1-10** did not show substantially higher antibacterial activity than NeoB against WT bacteria, we decided to directly assess the potential RNase activity of these compounds by using gel electrophoresis experiments as previously reported for ColE3^[20]. We envisioned that by incubating the designer structures with either the complete 70S ribosomes, the isolated 30S ribosomal particles, and/or the synthetic A-site oligonucleotide model structures, we could determine whether the new compounds have catalytic activity.

Initially, the experiments were performed on full-size ribosomes isolated from *E. coli* as previously reported^[35]. As a positive control, we used the RNase domain of the natural toxin ColE3 obtained from Prof. Colin Kleantous from Oxford University (Figure 3, panel B). As expected, with ColE3 we observed the cleavage of ~40 bases from the 16S rRNA fragment

(~1540 nucleic bases) in a dose-dependent manner. Figure 3 also shows the 5S and tRNA fragments. However, the experiments with NeoB and compound **3** (Figure 3, panels C and D) did not show any signs of the cleaved product at concentrations up to 400 μM . At higher concentrations, we encountered solubility problems, which prevented us from detecting RNA cleavage. At the same concentration range (up to 400 μM), ethylenediamine (a negative control) did not cleave the full ribosome (Figure 3, panel A), suggesting that it is unable to bind to rRNA effectively.

To avoid precipitation and allow the use of higher concentrations of aminoglycosides, instead of ribosomal particles, we decided to use an A-site oligonucleotide model. We selected an oligonucleotide model similar to that used by Westhof and co-workers^{[36],[37]} for crystallographic studies. To improve the RNA detection, we added a fluorescent tag Cy3 at the 3' end (and not at 5' end) in order to ensure that there is a significant difference between the size of the full length RNA and the cleaved RNA (see Figure S2 in Supporting Information). The cleavage experiments indicated that with the ethylenediamine (N-2-N) we observe nonspecific cleavages only at high concentrations, 100 and 200 μM of N-2-N (Figure 4, panel A).

In the presence of compound **6**, we detected some RNA cleavage at substantially lower concentrations, 10 μM (Figure 4, panel B). We observed the double-strand RNA (DS band in panel B) suggesting that the aminoglycoside binding stabilizes the double-stranded RNA even though the gel was under denaturing conditions. In addition, only nonspecific cleavage bands were observed at the concentrations tested which are far longer fragments than expected for a specific and selective cleavage (less than 8 bases).

All in all, we conclude that the initial NeoB derivatives (compounds **1-10**) that we designed and tested, exhibit significant

For internal use, please do not delete. Submitted_Manuscript

FULL PAPER

antibacterial activity and overcome existing resistance to aminoglycosides, however they lack any significant catalytic activity as we would have expected according to our initial design strategy.

2.6. MD simulations

2.6.1. Conformational dynamics of the warheads and the possibility of RNA cleavage

In an attempt to explain the experimental data of the newly designed compounds **1-10** at the molecular level, we performed full-atom molecular dynamics (MD) followed by Gaussian accelerated MD (GaMD)^{[38],[39]}. The crystal structure of NeoB bound to the oligonucleotide model of the A-site rRNA (PDB code: 2ET4)^[19] was used as a template for building the systems used in the simulations (for details see Simulation Methods in Supporting Information, Figure S6). Four representative derivatives of NeoB, compounds **2**, **5**, **8** and **10**, were simulated and NeoB was used as a control. Total MD and GaMD simulation time was about 5.5 μ s.

For compounds **2** and **5**, we found two and three different conformations of the warheads, respectively (Figures S3 and S4). For both, the dominant conformation of the warhead (82.7% of the population in **2**, and 76.4% of the population in **5**) is characterized by a common intra-molecular hydrogen bond between the N1 amine of the warhead), and the N6' ammonium of the aminoglycoside ring I. Unfortunately, these intra-molecular hydrogen bonds prevent the N1 amine of the warhead from acting as the general base to activate 2'-OH of the G1491 ribose as a nucleophile (see Figure 2 for the proposed mechanism).

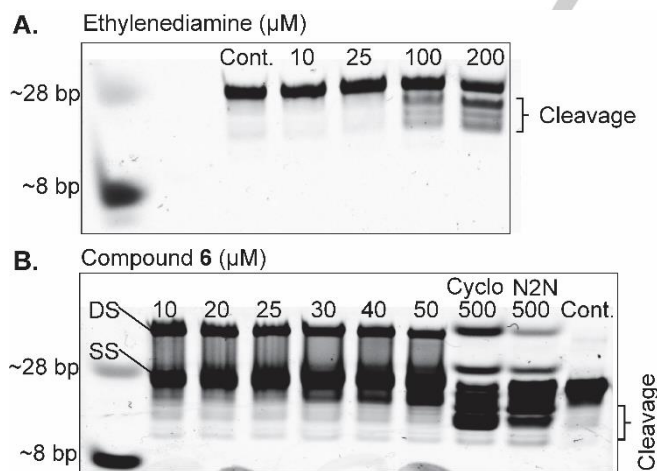


Figure 4. Cleavage experiments of the A-site oligonucleotide model rRNA (23 bases labeled at 3' with the fluorescent Cy3 tag, incubated for 24 hr, pH 8, 37 °C; for the sequence of rRNA see Figure S2 in Supporting Information) in the presence of ethylenediamine and compound **6**. A) Lane 1, RNA markers; Lane 2, blank lane; Lane 3, not treated (control); Lanes 4-7, rRNA oligonucleotide treated with increased concentrations of ethylenediamine. B) Lane 1, RNA markers; Lanes 2-7, rRNA oligonucleotide treated with increased concentrations of compound **6**; Lanes 8 and 9, rRNA oligonucleotide treated with 500 μ M 1,2-cyclohexane diamine (Cyclo) and ethylenediamine (N2N), respectively; Lane 10, not treated (control). rRNA fragments were analyzed on 20% TBE/urea gel and visualized by fluorescence. DS, double stranded rRNA. SS, single stranded rRNA.

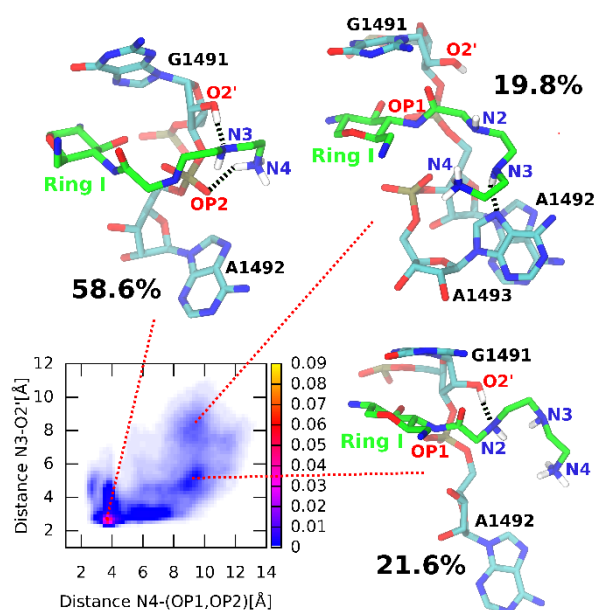


Figure 5. The normalized occurrence of the three binding modes of compound **8** warhead to A site as a function of the two intermolecular distances N3-O2' and N4-(OP1, OP2). The representative structures are presented. For clarity, only ring I of the aminoglycoside (in green) and hydrogen atoms crucial for interactions of the warhead are shown. Black dashed lines denote donor-acceptor short-range interactions.

In contrast to **2** and **5**, the warhead of **8** and **10**, which represent the 4'- and 6'-amide derivatives of NeoB, is longer and does not form any similar intra-molecular interactions with the rest of the molecule (Figure 5 and Figure S5). For compound **10** (Figure S5), we observed that the largest conformational variability of the warhead is associated with its rotation around the dihedral angle N2-C3-C4-N3. Therefore, we used this coordinate in the clustering analysis and found two major conformations of the warhead (72.2 % and 27.8% of the population). The short-range contacts of the N4' ammonium with the phosphates of A1492 and A1493 conformationally restrict not only the position of ring I in the A site but also the A1492 and A1493 backbone atoms.

For compound **8**, we identified three principal modes of binding of the warhead to the rRNA (Figure 5). In the most abundant binding mode (58.6% of the population), we observed two short-range interactions between the 2'-hydroxyl of the ribose (G1491) and the N3 amine of compound **8** (proposed general base) and between the A1492 phosphate and the N4 ammonium of compound **8** (general acid). Importantly, this conformational state of compound **8** is consistent with the hypothetical mechanism of the A-site rRNA cleavage between G1491 and A1492 (Figure 2). In the second most abundant binding mode of compound **8** (21.6% of the population), the N2 amine hydrogen bonds with the 2'-hydroxyl of the ribose of G1491, which actually now serves as the general base. However, the concomitant stabilization of the transition state via the interaction of the

For internal use, please do not delete. Submitted_Manuscript

FULL PAPER

warhead amines with the phosphate of A1492 is lacking, which would significantly limit the efficiency of hydrolysis.

Considering the formation of the interactions required for the A-site rRNA cleavage between G1491 and A1492, compound **8** seems the best candidate among the selected derivatives for the development of a catalytic antibiotic. The N3 amine of the warhead activates the 2'-OH of the G1491 ribose for the nucleophilic attack and the N4 ammonium of the warhead favorably binds to the OP2 and O3' atoms of the A1492 phosphate, facilitating the nucleophilic attack. However, the warhead hardly interacts with the O5' atom and consequently the activation of the leaving group would be minimal. We therefore predict that elongating the warhead might be beneficial so that the N4 ammonium could interact with the A1492 phosphate-leaving group more directly and frequently.

In general, the efficiency of rRNA hydrolysis is highly dependent on the ability of the catalyst to induce the correct positioning of the nucleophile for in-line attack on the scissile bond. Enzymes, being large, can mechanically achieve this step 'easily' by distorting the substrate to reach the conformation necessary for efficient catalysis. For example, ColE3^[20] and α -sarcin^[40], the two bacterial toxins that cleave a single phosphodiester bond of rRNA (in the small and in the large ribosomal subunit, respectively), both use RNA base flipping in order to dock the substrate into the active site in such a manner as to facilitate the crucial in-line attack. Whether the aminoglycoside-warhead combination can induce a similar conformational change of the rRNA A-site is one of the most important questions of this work. To address this question, we measured the angle created between the 2'-OH (the G1491 ribose, the nucleophile), the phosphorus of the phosphate between G1491 and A1492, and the 5'O (the leaving group) – O–P–O angle.

In the crystal structure of the Westhof model that we used for the simulations, the O–P–O angle does not exceed 90 degrees. Figure 6 compares the distribution of the O–P–O angle as obtained from GaMD simulations of NeoB, and its derivatives **2**, **5**, **8** and **10**. The smallest values of this angle are found for the NeoB complex, distributed in the range of 45–105 degrees. The interactions formed between O3' of NeoB (ring I) and OP2 of the A1492 phosphate, and between O4' of NeoB (ring I) and OP2 of the A1493 phosphate seem to be the most important for the O–P–O angle orientation. The modifications introduced into the NeoB ring I to make compounds **8** and **10**, clearly led to the increase of this angle for both derivatives, reaching as high as 170 degrees for **10**. We found that for the nearly linear orientation of the O–P–O angle, a strong and stable interaction with the OP1 atom of the A1492 phosphate is essential. For compound **8**, this requirement is fulfilled thanks to the persistent hydrogen bond formed by the 3'-hydroxyl of ring I and concomitant stabilization of the A1492 phosphate by the N4 ammonium of the warhead. For compound **10**, the crucial short-range interaction with the OP1 atom of the A1492 phosphate is made by the N4' ammonium in ring I. Even though the warhead of compound **10** does not reach the putative rRNA cleavage site, the stabilization of the –O–P–O angle in the nearly in-line orientation is remarkable. Thus, we believe that using flexible docking algorithms, the structure of the warhead of compound **10** can be remodeled to optimize its ability to form the

interactions necessary to cleave the rRNA. Therefore, together with compound **8**, we consider **10** as a lead compound for the next generation of new aminoglycoside derivatives that are designed to achieve rRNA catalysis.

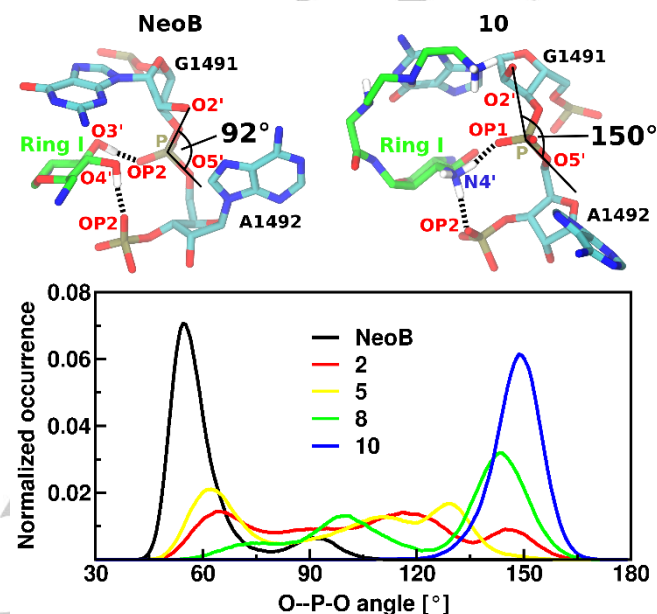


Figure 6. The distribution of the O–P–O angle for NeoB and compounds **2**, **5**, **8** and **10** in GaMD simulations. The inset shows the O–P–O angle in the representative structures of NeoB and compound **10**. The donor-acceptor short-range interactions important for stabilization of the O–P–O angle are marked by black dashed lines. For clarity, only ring I of the aminoglycosides (in green) and selected hydrogen atoms are shown.

2.7 Summary and Conclusions

We adopted the idea of catalytic antibiotics from nature: bacteria produce bacteriocins that exert their lethal action by an enzymatic nuclease digestion mechanism. Based upon the most recent structural and mechanistic data on the bacteriocin ColE3 and on the aminoglycoside antibiotics, we have designed and synthesized a series of aminoglycosides bearing a potential catalytic moiety, with the expectation that these molecules could mimic ColE3 activity. Our design principles included a careful analysis of the choice of the 'target' phosphodiester bond, the 'catalytic warhead' structures, and the attachment site on the aminoglycoside scaffold. We selected the phosphodiester bond between the rRNA bases G1491 and A1492 as the potential cleavage site, the 4'-OH group (ring I) of the natural aminoglycoside NeoB as an attachment site for the catalytic warheads, and by attaching a series of different 1,2-diamines as potential catalytic warheads we prepared the new NeoB derivatives (compounds **1-10**, Figure 1).

To probe the influence of the attached warheads on antibacterial activity, the derivatives **1-10** were tested against WT, pathogenic and aminoglycoside resistant strains (Table 1). In general, the compounds **2-10** showed significant antibacterial

For internal use, please do not delete. Submitted_Manuscript

FULL PAPER

activity against WT bacteria, which was similar to or slightly lower than that of the parent NeoB. The observed antibacterial data was corroborated by the *in vitro* protein translation inhibition data (IC50 values, Table 1) showing activity similar to that of the parent NeoB. Of particular note is the potent antibacterial activity of the new derivatives (versus that of NeoB) against resistant and pathogenic strains like *P. aeruginosa* and MRSA, with the lead compounds exhibiting MIC values 8-16 times lower in *P. aeruginosa* (compound **6**) and 64 times lower in MRSA (compounds **2** and **8**).

We anticipated that unusually low MIC and IC50 values against WT bacteria would be indicative of significant catalytic activity on the ribosomal RNA, but in this regard the observed data was not encouraging. However, these data alone cannot conclusively disprove the desired hydrolytic activity, since they could also be explained by a low catalytic turnover resulting from strong binding affinity of the derivative to the cleaved rRNA.

To address whether the new derivatives exhibit the anticipated hydrolytic activity, we tested the comparative RNase activity using full-size ribosomes isolated from *E. coli* (Fig. 3) and the bacterial A-site oligonucleotide model RNA (Fig. 4). In the *E. coli* ribosomes, we confirmed the reported activity of the ColE3 as the positive control. However, neither NeoB nor compound **3** showed any activity at concentrations of up to 400 μM ; at higher concentrations, we encountered solubility problems. The cleavage experiments with the A-site oligonucleotide model RNA indicated weak, dose dependent but nonspecific hydrolytic cleavage activity for compound **6**. Although other RNA models could be employed that would more precisely monitor strand cleavage (e.g. the use of ^{32}P end-labeled A-site RNA construct^[41]), it is clear that if the new derivatives would exhibit the desired function at an appreciable level, the experiments we performed would certainly detect them. In view of these discouraging results, it is prudent to consider whether or not there is sufficient justification to encourage further research towards catalytic aminoglycosides and if so then what should be the next step?

The observed similar MIC and IC50 values of **2-10** to those of NeoB against WT bacteria indicated that the modifications on NeoB have not hindered the bacterial cell permeability or the binding affinity of the aminoglycoside scaffold to the target site. Furthermore, full-atom GaMD simulations (Fig. 6) on the crystal structure of NeoB bound to the oligonucleotide model of the A-site rRNA revealed that the O—P—O angle for compounds **8** and **10** is significantly greater than that of NeoB (between 45 and 105 degrees), reaching as high as 170 degrees for **10**, which is remarkably close to the ideal, in-line orientation of nucleophilic attack. These data support the notion that appropriately designed aminoglycoside-warheads such as **8** or **10**, have the capacity 1) to bind selectively to the regular aminoglycoside binding site and 2) to induce the conformational changes that are necessary to lower the activation barrier of the transition state for hydrolytic cleavage. Taken together, these results suggest that using flexible docking algorithms, the structures of the warheads in compounds **8** and **10** could be re-modelled to optimize their ability to catalytically cleave the rRNA.

In summary, this pilot study provides a new direction for the development of novel aminoglycoside-based small molecules that target bacterial rRNA by means of optimizing the efficacy of

aminoglycoside-induced rRNA cleavage; this progress may offer promise for the development of catalytic antibiotics as a new paradigm in antibiotics research. Thus, although 'the catalytic aminoglycoside' is yet to be found, the results introduced in this study indicate that this is an achievable goal. More comprehensive design strategies are now being employed, which incorporate advanced molecular dynamics techniques and more powerful metal-free and metal-based catalytic warheads, to optimize the catalytic activity of the new designer structures.

3. Experimental Section

Experimental Details. 3.1. General Techniques: NMR spectra (including ^1H , ^{13}C , DEPT, 2D-COSY, 1D TOCSY, HMQC, HMBC) were routinely recorded on a Bruker Avance™ 500 spectrometer, and chemical shifts reported (in ppm) are relative to internal Me_4Si ($\delta=0.0$) with CDCl_3 as the solvent, and to MeOD ($\delta=3.35$) as the solvent. ^{13}C NMR spectra were recorded on a Bruker Avance™ 500 spectrometer at 125.8 MHz, and the chemical shifts reported (in ppm) relative to the solvent signal for CDCl_3 ($\delta=77.00$), or to the solvent signal for MeOD ($\delta=49.0$). Mass spectra analyses were obtained either on a Bruker Daltonix Apex 3 mass spectrometer under electron spray ionization (ESI) or by a TSQ-70B mass spectrometer (Finnigan Mat). Reactions were monitored by TLC on Silica Gel 60 F₂₅₄ (0.25 mm, Merck), and spots were visualized by charring with a yellow solution containing $(\text{NH}_4)_2\text{Mo}_7\text{O}_{24}\cdot 4\text{H}_2\text{O}$ (120 g) and $(\text{NH}_4)_2\text{Ce}(\text{NO}_3)_6$ (5 g) in 10% H_2SO_4 (800 mL). Flash column chromatography was performed on Silica Gel 60 (70-230 mesh). All reactions were carried out under an argon atmosphere with anhydrous solvents, unless otherwise noted. Neomycin B and Paromomycin as analytical samples for comparative biochemical assays were purchased from Sigma. For the chemical synthesis, large scale Paromomycin (used as a starting material) was purchased from Apollo Scientific LTD (SK6 2QR United Kingdom). All other chemicals and biochemicals, unless otherwise stated, were obtained from commercial sources. In all biological tests, all the tested aminoglycosides were in their sulfate salt forms except compound **5**, which was used as its trifluoroacetate salt.

3.2. Biochemical assays: Prokaryotic *in-vitro* translation inhibition by the different standard and synthetic aminoglycosides was quantified in coupled transcription/translation assays by use of *E. coli* S30 extract for circular DNA with the pBEST/*luc*™ plasmid (Promega), according to the manufacturer protocol. Translation reactions (25 μL) containing variable concentrations of the tested aminoglycoside were incubated at 37 °C for 60 min, cooled on ice for 5 min, and diluted with a dilution reagent (tris-phosphate buffer (25 mM, pH 7.8), DTT (2 mM), 1,2-diaminocyclohexanetetraacetate (2 mM), glycerol (10%), triton x100 (1%) and BSA (1 mg/mL)) into 96-well plates. The luminescence was measured immediately after the addition of Luciferase Assay Reagent (Promega) (50 μL), and light emission was recorded with Victor3™ Plate Reader (Perkin-Elmer). The concentration of half-maximal inhibition (IC₅₀) was obtained from fitting concentration-response curves to the data of at least three independent experiments, using Grafit 5 software^[42].

Comparative antibacterial activities were determined by measuring the MIC values using the double-microdilution method according to the National Committee for Clinical Laboratory Standards (NCCLS)^[43]. All the experiments were performed in triplicates and analogous results were obtained in three different experiments.

For the rRNA cleavage experiments, the ribosomes were isolated from *E. coli* cells (R477-100) by following the reported protocol.^[35] Ribosomes are

For internal use, please do not delete. Submitted_Manuscript

FULL PAPER

pelleted from pooled fractions (35 K for 15 h at 4°C) and resuspended in buffer for snap freezing in liquid nitrogen and storage at -80 °C. The resin is rinsed with water after use and stored in 20% ethanol at 4°C. The catalytic domain of ColE3 (provided by Prof. Kleanthous) was purified from its immunity protein as previously described^[44]. Briefly, after elution from the Ni-affinity column with 6M GnHCl, the ColE3 RNase becomes unfolded. It refolds upon dialysis into 50 mM potassium phosphate or 20 mM Tris pH 7.5 buffer. All the purification procedure can be carried out at room temperature and the product was analyzed on 16% SDS-PAGE.

The cleavage experiments of rRNA with *E. coli* ribosomes were performed by incubation of freshly isolated ribosomes for 24 h (5 minutes in case of ColE3) (37°C, pH 7.0) in the presence of ethylenediamine, NeoB compound **3** or ColE3. After incubation, RNA was phenol/chloroform extracted from samples and electrophoresed on a 6% acrylamide TBE/urea gel for 100 min at 180 V, stained with syber gold, and analyzed by fluorescence. Short RNA oligomer that represents the bacterial A-site sequence labeled with fluorescent tag (23 bases, for sequence see Figure S2) was also used for rRNA cleavage experiments. This RNA sequence was purchased from Dharmacon and was used without further purification. The cleavage experiments were performed by using gel electrophoresis; the rRNA fragments were analyzed on 20% TBE/urea gel and visualized by fluorescence.

3.3. Molecular dynamics simulations. MD simulations were carried out on the model of the A site containing two symmetric aminoglycoside binding sites using the crystal structure of the A site with neomycin B bound (PDB code: 2ET4)^[19]. The MD simulation protocol consisted of energy minimization, thermalization, equilibration, and production phases. In the first two phases, harmonic constraints with the force constant of 10 kcal/mol/Å² were imposed on heavy atoms of the solute. First, all systems were energy minimized with the above restraints undergoing 5000 steps of steepest descent followed by 4000 steps of conjugate gradient minimization using *sander* (Amber 12). The next phases were carried out with NAMD^[45]. Second, during thermalization (in the NVT ensemble), each system was heated from 10 to 310 K increasing the temperature by 10 K every 100 ps. Then 2 ns simulations at 310 K were carried out. Third, equilibration was performed in the NpT ensemble with a constant pressure of 1 atm controlled using Langevin Piston method and at constant temperature of 310 K regulated by Langevin dynamics with a damping factor of 1 ps⁻¹. During 5 ns equilibration the restraints were exponentially decreased in 50 time windows (scaled from 1 to 0.0065). Further, the 120 ns production runs were performed without any restraints. Periodic boundary conditions and Particle Mesh Ewald method with grid spacing of 1 Å were used. The SHAKE algorithm and the integration time step of 2 fs were applied. For non-bonded interactions a short-range cutoff of 12 Å was used.

After the above MD production phase, the GaMD simulation^[39],^[39] started with another 2 ns MD simulation to gather the statistics of the potential energy of the system in order to calculate the GaMD acceleration parameters. After adding the boost potential, the simulation was continued for 30 ns to equilibrate the system. Subsequently, ten independent GaMD production runs were conducted for 100 ns each starting with randomized initial atomic velocities. The GaMD simulations were performed in the dual-boost mode in which the boost potential is applied to the dihedral and total potential energy terms. The threshold energy was set to the lower bound, i.e., $E = V_{\max}$. The upper limit of the boost potential standard deviation, σ_0 , was set to 10 kcal/mol for the dihedral and total potential energetic terms.

Acknowledgements

The authors thank Prof. Colin Kleanthous from Oxford University for providing ColE3 toxin, Dr. Eli Shulman for performing the initial RNase tests by gel electrophoresis, and Dr. Moran Shalev for helping in the initial design and modelling experiments. This work was supported by research grants from the Israel Science Foundation founded by the Israel Academy of Sciences and Humanities (grant no. 1845/14 for TB), from the Ministry of Science, Technology and Space, State of Israel (grant no. 2022675 for TB), by the Interdisciplinary Centre for Mathematical and Computational Modelling University of Warsaw (grants G31-4, GA65-16, GA73-21 for JT and TP) and by the National Science Centre, Poland (UMO-2017/26/M/NZ1/00827). J. T. acknowledges the Polish-U.S. Fulbright Commission. V.B. acknowledges the financial support by the Ministry of Immigration Absorption and the Ministry of Science and Technology, Israel (Kamea Program).

Conflicts of interest

The authors declare no conflict of interest.

Keywords: Aminoglycosides • Catalytic Antibiotic • RNA Cleavage • Bacterial Ribosome • Decoding A-site

- [1] B. Bozdogan, L. Ednie, K. Credito, K. Kosowska, P. C. Appelbaum, *Antimicrob. Agents Chemother.* **2004**, *48*, 4762–4765.
- [2] B. I. Eisenstein, *Expert Opin. Investig. Drugs* **2004**, *13*, 1159–1169.
- [3] V. Pokrovskaya, I. Nudelman, J. Kandasamy, T. Baasov, *Aminoglycosides. Redesign Strategies for Improved Antibiotics and Compounds for Treatment of Human Genetic Diseases*, **2010**.
- [4] J. Suh, W. S. Chei, *Curr. Opin. Chem. Biol.* **2008**, *12*, 207–213.
- [5] Z. Yu, J. A. Cowan, *Chem. - A Eur. J.* **2017**, *23*, 14113–14127.
- [6] T. Niittymaki, H. Lonnberg, *Org. Biomol. Chem.* **2006**, *4*, 15–25.
- [7] T. Lönnerberg, K. M. Kero, *Org. Biomol. Chem.* **2012**, *10*, 569–574.
- [8] R. Salvio, R. Cacciapaglia, L. Mandolini, F. Sansone, A. Casnati, *RSC Adv.* **2014**, *4*, 34412–34416.
- [9] S. Magnet, J. S. Blanchard, *Chem. Rev.* **2005**, *105*, 477–498.
- [10] A. Sreedhara, A. Patwardhan, J. A. Cowan, *Chem. Commun.* **1999**, *2*, 1147–1148.
- [11] A. Patwardhan, J. A. Cowan, *Dalt. Trans.* **2011**, *40*, 1795–1801.
- [12] W. Szczepanik, A. Krezel, M. Brzezowska, E. Dworniczek, M. Jezowska-Bojczuk, *Inorganica Chim. Acta* **2008**, *361*, 2659–2666.
- [13] W. Szczepanik, J. Ciesiolka, J. Wrzesiński, J. Skala, M. Jezowska-Bojczuk, *Dalt. Trans.* **2003**, 1488–1494.
- [14] W. Szczepanik, E. Dworniczek, J. Ciesiolka, J. Wrzesiński, J. Skala, M. Jezowska-Bojczuk, *J. Inorg. Biochem.* **2003**, *94*, 355–364.
- [15] S. M. K. Takahashi, *Acad. Press. New York* **1982**, 435–468.
- [16] X. J. Yang, T. Gerczei, L. Glover, C. C. Correll, *Nat. Struct. Biol.* **2001**, *8*, 968–973.
- [17] P. B. Rupert, A. R. Ferre-D'Amare, *Nature* **2001**, *410*, 780–786.
- [18] C. L. Ng, K. Lang, N. A. G. Meenan, A. Sharma, A. C. Kelley, C. Kleanthous, V. Ramakrishnan, *Nat. Struct. Mol. Biol.* **2010**, *17*,

For internal use, please do not delete. Submitted_Manuscript

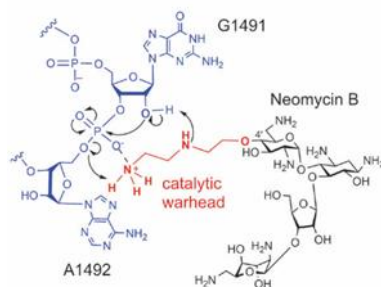
FULL PAPER

- 1241–1246.
- [19] B. François, R. J. M. Russell, J. B. Murray, F. Aboul-ela, B. Masquida, Q. Vicens, E. Westhof, *Nucleic Acids Res.* **2005**, *33*, 5677–5690.
- [20] C. L. Ng, K. Lang, N. A. G. Meenan, A. Sharma, *Nat. Struct. & Mol. Biol.* **2010**, DOI 10.1038/nsmb.1896.
- [21] M. Komiyama, K. Yoshinari, *J. Org. Chem.* **1997**, *62*, 2155–2160.
- [22] K. Yoshinari, M. Komiyama, *Chem. Lett.* **1990**, 519–522.
- [23] R.-B. B. Yan, M. Yuan, Y. F. Wu, X. F. You, X.-S. S. Ye, *Bioorg. Med. Chem.* **2011**, *19*, 30–40.
- [24] K. C. Nicolaou, V. a. Adsool, C. R. H. Hale, *Org. Lett.* **2010**, *12*, 1552–1555.
- [25] N. S. Chindarkar, A. H. Franz, *Arkivoc* **2008**, *2008*, 21.
- [26] R. Pathak, D. Perez-Fernandez, R. Nandurdikar, S. K. Kalapala, E. C. Bottger, A. Vasella, *Helv. Chim. Acta* **2008**, *91*, 1533–1552.
- [27] R. Pathak, E. C. C. Böttger, A. Vasella, *Helv. Chim. Acta* **2005**, *88*, 2967–2985.
- [28] E. D. Goddard-borger, R. V. Stick, **2007**, 7515–7517.
- [29] V. Pokrovskaya, V. Belakhov, M. Hainrichson, S. Yaron, T. Baasov, *J. Med. Chem.* **2009**, *52*, 2243–2254.
- [30] J. Kondo, M. Hainrichson, I. Nudelman, D. Shallom-Shezifi, C. M. C. M. Barbieri, D. S. D. S. Pilch, E. Westhof, T. Baasov, *ChemBioChem* **2007**, *8*, 1700–1709.
- [31] M. T. G. Holden, E. J. Feil, E. Al., *Proc. Natl. Acad. Sci.* **2004**, *101*, 9786–9791.
- [32] G. Kaneti, H. Sarig, I. Marjeh, Z. Fadia, A. Mor, *FASEB J.* **2013**, *27*, 4834–43.
- [33] J. I. Sekiguchi, T. Asagi, T. Miyoshi-Akiyama, T. Fujino, I. Kobayashi, K. Morita, Y. Kikuchi, T. Kuratsuji, T. Kirikae, *Antimicrob. Agents Chemother.* **2005**, *49*, 3734–3742.
- [34] M. Hainrichson, O. Yaniv, M. Cherniavsky, I. Nudelman, D. Shallom-Shezifi, S. Yaron, T. Baasov, *Antimicrob. Agents Chemother.* **2007**, *51*, 774–776.
- [35] B. a. Maguire, L. M. Wondrack, L. G. Contillo, Z. Xu, *RNA* **2008**, *14*, 188–195.
- [36] P. Pfister, S. Hobbie, Q. Vicens, E. C. Böttger, E. Westhof, *ChemBioChem* **2003**, *4*, 1078–1088.
- [37] Q. Vicens, E. Westhof, *Chem. Biol.* **2002**, *9*, 747–755.
- [38] Y. Miao, V. A. Feher, J. A. McCammon, *J. Chem. Theory Comput.* **2015**, *11*, 3584–3595.
- [39] Y. T. Pang, Y. Miao, Y. Wang, J. A. McCammon, *J. Chem. Theory Comput.* **2017**, *13*, 9–19.
- [40] C. C. Correll, X. Yang, T. Gerczei, J. Beneken, M. J. Plantinga, *J. Synchrotron Radiat.* **2004**, *11*, 93–96.
- [41] M. J. Belousoff, B. Graham, L. Spiccia, Y. Tor, *Org. Biomol. Chem.* **2009**, *7*, 30–33.
- [42] Leatherbarrow, R. J. GraFit 5; Erithacus Software Ltd.: Horley, U.K., 2001.
- [43] NCCLS, *National Committee for Clinical Laboratory Standards, Performance Standards for Antimicrobial Susceptibility Testing. Fifth Information Supplement: Approved Standard M100-S5*, NCCLS, Villanova, Pa., **1994**.
- [44] S. Carr, D. Walker, R. James, C. Kleanthous, A. M. Hemmings, *Structure* **2000**, *8*, 949–960.
- [45] J. C. Phillips, R. Braun, W. Wang, J. Gumbart, E. Tajkhorshid, E. Villa, C. Chipot, R. D. Skeel, L. Kalé, K. Schulten, *J. Comput. Chem.* **2005**, *26*, 1781–1802.

FULL PAPER

FULL PAPER

Text for Table of Contents

*Author(s), Corresponding Author(s)****Page No. – Page No.****Title**

Accepted Manuscript